Physica E 85 (2017) 143–151

Contents lists available at ScienceDirect

Physica E

journal homepage: www.elsevier.com/locate/physe

Provide a suitable range to include the thermal creeping effect on slip velocity and temperature jump of an air flow in a nanochannel by lattice Boltzmann method

Arash Karimipour

Department of Mechanical Engineering, Najafabad Branch, Islamic Azad University, Najafabad, Iran

ARTICLE INFO

Article history:
Received 24 May 2016
Received in revised form
12 July 2016
Accepted 17 August 2016
Available online 22 August 2016

Keywords:
Lattice Boltzmann method
Nanochannel
Thermal creeping
Slip flow

ABSTRACT

The thermal creeping effect on slip velocity of air forced convection through a nanochannel is studied for the first time by using a lattice Boltzmann method. The nanochannel side walls are kept hot while the cold inlet air streams along them. The computations are presented for the wide range of Reynolds number, Knudsen number and Eckert number while slip velocity and temperature jump effects are involved. Moreover appropriate validations are performed versus previous works concerned the micro–nanoflows.

The achieved results are shown as the velocity and temperature profiles at different cross sections, streamlines and isotherms and also the values of slip velocity and temperature jump along the nanochannel walls. The ability of the lattice Boltzmann method to simulate the thermal creeping effects on hydrodynamic and thermal domains of flow is shown at this study; so that its effects should be involved at lower values of Eckert number and higher values of Reynolds number especially at entrance region where the most temperature gradient exists.

1. Introduction

Micro and NanoElectro Mechanical Systems (MEMS and NEMS) are considered as the one of main favorite research topics nowadays. Flow properties in microscale regimes are different from the macro ones; so that well known Knudsen number ($Kn=\lambda/D_H$) is used to classify the micro–nanoflows where λ represents the molecular mean free path. The fluid flow is supposed as continuum at $Kn<0.001$ and Navier–Stokes equations could be used to simulate the flow field at this state [1–5]. However other regimes as like the slip flow, transient and free molecular can be achieved at $0.001<Kn<0.1$, $0.1<Kn<10$ and $Kn>10$, respectively [6–11].

Navier–Stokes methods with slip velocity boundary condition beside the particle based methods are able to investigate the slip flow regime. The trace and collision between the molecular and particles of a gas flow are the main objects of particle based methods including lattice Boltzmann method (LBM), direct simulation of Monte Carlo (DSMC) and molecular dynamics (MD) [12–16]. Among them, LBM shows less cost of computation and also works with simpler math equations than MD or DSMC which makes LBM more functional for the microflows [17–22].

LBM consists of collision and propagation between the particles placed on the specified locations on a lattice. In this approach, the fluid domain is considered by the fictive particles which each one has been made of too many molecular. LBM is almost a new model which deals better with the complex boundaries than the CFD methods. Moreover LBM uses the simple and parallel algorithm that can be used for a wide range of Knudsen number [23–28]. However it should be mentioned that LBM needed an appropriate collision operation to avoid divergence; in this way, the model of LBM-BGK was developed which showed suitable accuracy and stability [29–31].

Different models of thermal LBM can be referred for the thermal domains. The internal energy distribution function one is able to consider the pressure work and viscous heat dissipation beside its higher numerical stability. This approach is called thermal lattice Boltzmann method (TLBM) which the both of hydrodynamic (f) and thermal (g) distribution functions are used in together [32–38].

Provide a suitable formulation for the boundary conditions in terms of distribution functions is one of disadvantages of LBM so that several researchers are trying to develop the useful practical LBM-boundary conditions. Diffuse scattering boundary condition (DSBC) introduced by Niu et al. [39,40] and Shu et al. [41] represents the relaxation time according to the Knudsen number to determine the slip velocity.

E-mail address: arashkarimipour@gmail.com

http://dx.doi.org/10.1016/j.physe.2016.08.021
1386-9477/

Nomenclature

AR=L/H=30 velocity in microscopic scale
c=(c_x,c_y) velocity in microscopic scale
c_s the speed of sound in lattice unit
D_H=$2H$ hydraulic diameter (m)
Ec=$\mathrm{Ma}^2(k-1)T_0/\Delta T$ Eckert number
f, g momentum and internal energy distribution functions
$\tilde{f}_i$, $\tilde{g}_i$ modified distribution functions
H, L nanochannel height and length (m)
k ratio of specific heats
Kn=λ/D_H Knudsen number
Ma Nusselt number
Nu Nusselt number
Pr=υ/α Prandtl number
Re=$\rho_i u_i D_H/\mu$ Reynolds number
t time (s)
T temperature (K)
$\mathbf{u}$=(u,v) velocity vector in macroscopic scale, (m s^{-1})
(U,V)=(u/u_i,v/u_i) dimensionless macroscopic velocity
U_s dimensionless slip velocity
x, y cartesian coordinates (m)
(X,Y)=(X/H,Y/H) dimensionless Cartesian coordinate
Z heat dissipation

Greek symbols

λ molecular mean free path
υ kinematic viscosity (m^2/s)
θ=($T-T_C$)/(T_H-T_C) dimensionless temperature
θ_s dimensionless temperature jump
ρ density (kg m^{-3})
μ dynamic viscosity (Pa s)
τ_f, τ_g momentum and internal energy relaxation times

Super- and sub-scripts

C cold
e equilibrium
H hot
i the link number of lattice, Inlet flow
w wall

There are several other different models in this way and it is still tried to develop LBM ability at different geometries and conditions [42–48]. However the effect of thermal creeping has been ignored in the majority of them; hence there is lack of works concerned this phenomenon which means less accuracy in achievements. As a result, the effect of thermal creeping on hydrodynamic and thermal properties of a nanoflow is provided by LBM for the first time at present work.

2. Problem statement

Forced convection of air (Pr=υ/α=0.7) through a two dimensional nanochannel is studied numerically by using the lattice Boltzmann method (Fig. 1). TLBM-BGK model based on momentum (f) and internal energy (g) distribution functions is chosen to simulate the flow and heat transfer at $0.001 \le \mathrm{Kn} \le 0.1$; which implies the slip flow regime at Reynolds number equals to Re=$\rho_i u_i D_H/\mu$=10,100,1000. The appropriate hydrodynamic and thermal boundary conditions are used in terms of distribution functions needed for LBM. The two dimensional-9 point lattice as D_2Q_9 is selected which is shown in Fig. 2 [18]. Nanochannel side walls are kept hot at T_H while the cold inlet air at T_C, streams along them. The nanochannel aspect ratio is supposed as AR=L/H=30. The width of channel is considered as H=250 nm which means the length equals to L=7.5 μm. Moreover the mean free path of the air molecules (λ) is almost equals to 50 nm. These facts imply why the authors called the expression of nanochannel to the supposed channel configuration at Kn=0.1. However the phrase of microchannel has been also used in the several previous works.

Present work aims to investigate the effect of thermal creeping on the flow and heat transfer of a nanoflow which has been

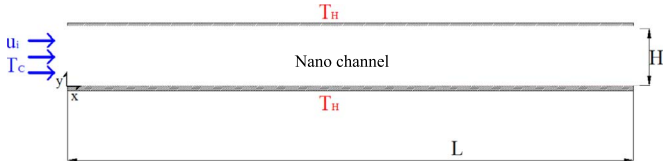

Fig. 1. The schematic figure of the nanochannel.

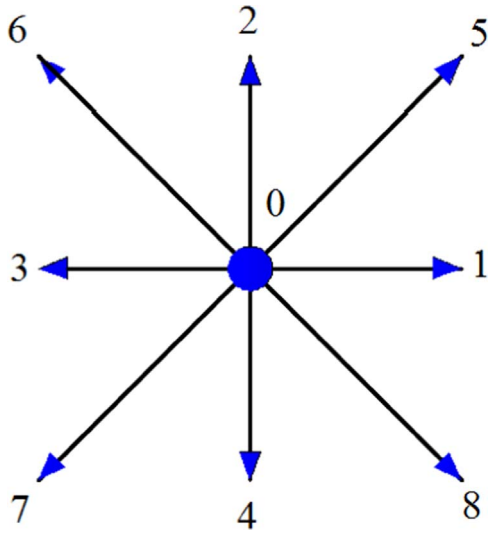

Fig. 2. D_2Q_9 lattice configuration.

ignored in the previous works. Moreover the effects of this phenomenon on slip velocity and temperature jump are studied. To do this, the wide range of Eckert number is selected at each section as $0.1 < \mathrm{Ec}=\mathrm{Ma}^2(k-1)T_0/\Delta T < 10$.

3. Numerical procedure

3.1. Lattice Boltzmann method

Using density-momentum distribution function, the Boltzmann equation is observed as [33]:

$$\partial_t f + (\mathbf{c}.\nabla)f = \Omega(f) \tag{1}$$

Ω is the collision operation. The internal energy distribution function is written as follows to simulate the thermal domain:

$$g = 0.5(\mathbf{c}-\mathbf{u})^2 f \tag{2}$$

which leads to generate the thermal lattice Boltzmann equation according to the internal energy:

$$\partial_t g + (\mathbf{c}.\nabla)g = \Omega(g) \tag{3}$$

Now the collision operations of LBM-BGK model for hydrodynamic and thermal fields are defined:

$$\Omega(f) = -\frac{f - f^e}{\tau_f} \tag{4}$$

$$\Omega(g) = -\frac{g - g^e}{\tau_g} - fZ = 0.5(\mathbf{c} - \mathbf{u})^2\Omega(f) - fZ \tag{5}$$

in which the heat dissipation term ($f Z$) can be determined as:

$$fZ = f(\mathbf{c} - \mathbf{u}).\left[\partial_t\mathbf{u} + (\mathbf{c}.\nabla)\mathbf{u}\right] \tag{6}$$

τ_f is the hydrodynamic relaxation time and also τ_g is the thermal relaxation time, respectively. Now the two new modified functions $\tilde{f}_i$ and $\tilde{g}_i$ are presented to avoid from implicitness in Eqs. (1)–(5):

$$\tilde{f}_i = f_i + \frac{dt}{2\tau_f}(f_i - f_i^e) \tag{7}$$

$$\tilde{g}_i = g_i + \frac{dt}{2\tau_g}(g_i - g_i^e) + \frac{dt}{2}f_i Z_i \tag{8}$$

The hydrodynamic and thermal Maxwell equilibrium distribution functions are shown as f_i^e and g_i^e, respectively. It is worth nothing that "i" demonstrates the lattice link number; hence Z_i can be written as follows:

$$Z_i = (\mathbf{c}_i - \mathbf{u}).D_i\mathbf{u} \text{ and } D_i = \partial_t + \mathbf{c}_i.\nabla \tag{9}$$

$$\mathbf{c}_i = \left(\cos\frac{i-1}{2}\pi,\ \sin\frac{i-1}{2}\pi\right)\mathbf{c},\ i = 1, 2, 3, 4$$
$$\mathbf{c}_i = \sqrt{2}\left(\cos\left[\frac{(i-5)}{2}\pi + \frac{\pi}{4}\right],\ \sin\left[\frac{(i-5)}{2}\pi + \frac{\pi}{4}\right]\right)\mathbf{c},$$
$$i = 5, 6, 7, 8\mathbf{c}_0 = (0, 0) \tag{10}$$

where the discrete microscopic velocity is stated by $\mathbf{c}_i$. Now the collision and propagation steps are performed by using f^e and g^e:

$$\tilde{f}_i(\mathbf{x} + \mathbf{c}_i dt, t + dt) - \tilde{f}_i(\mathbf{x}, t) = -\frac{dt}{\tau_f + 0.5dt}\left[\tilde{f}_i - f_i^e\right] \tag{11}$$

$$\tilde{g}_i(\mathbf{x} + \mathbf{c}_i dt, t + dt) - \tilde{g}_i(\mathbf{x}, t) = -\frac{dt}{\tau_g + 0.5dt}\left[\tilde{g}_i - g_i^e\right] - \frac{\tau_g dt}{\tau_g + 0.5dt}f_i Z_i \tag{12}$$

$$f_i^e = \omega_i\rho\left[1 + \frac{3\mathbf{c}_i.\mathbf{u}}{c^2} + \frac{9(\mathbf{c}_i.\mathbf{u})^2}{2c^4} - \frac{3(u^2 + v^2)}{2c^2}\right] \tag{13}$$

$$\begin{aligned} g_0^e &= -\omega_0\left[\frac{3\rho e}{2}\frac{u^2 + v^2}{c^2}\right]g_{1,2,3,4}^e \\ &= \omega_1\rho e\left[1.5 + 1.5\frac{\mathbf{c}_i.\mathbf{u}}{c^2} + 4.5\frac{(\mathbf{c}_i.\mathbf{u})^2}{c^4} - 1.5\frac{u^2 + v^2}{c^2}\right]g_{5,6,7,8}^e \\ &= \omega_2\rho e\left[3 + 6\frac{\mathbf{c}_i.\mathbf{u}}{c^2} + 4.5\frac{(\mathbf{c}_i.\mathbf{u})^2}{c^4} - 1.5\frac{u^2 + v^2}{c^2}\right] \end{aligned} \tag{14}$$

For D_2Q_9 model $\mathbf{c}^2 = 3RT = 1$ and the weight functions are chosen as $\omega_0 = 4/9$ and $\omega_i = 1/9$, $i = 1,2,3,4$ and $\omega_i = 1/36$, $i = 5,6,7,8$. As a result the macroscopic parameters can be determined as below, while $\rho e = \rho RT$:

$$\rho = \sum_i \tilde{f}_i\rho\mathbf{u} = \sum_i \mathbf{c}_i\tilde{f}_i\rho e = \sum_i \tilde{g}_i - \frac{dt}{2}\sum_i f_i Z_i \tag{15}$$

Based on gases kinetic theory, Knudsen number is achieved as follows:

$$\mathrm{Kn} = \sqrt{\frac{\pi k}{2}}\frac{\mathrm{Ma}}{\mathrm{Re}} \tag{16}$$

k is the heat capacity ratio of a gas. The amounts of relaxation times can be determined according to the definition of variables like Re, $\mathrm{Ma} = u_i/c_s$, $\tau = \mu/P$, $P = \rho c_s^2$ and $c_s = 1/3^{0.5}$:

$$\tau_f = \sqrt{\frac{6}{\pi k}}D_H.\,\mathrm{Kn} \tag{17}$$

$$\tau_g = \frac{\tau_f}{\mathrm{Pr}} \tag{18}$$

3.2. Boundary conditions

The non-equilibrium bounce back model is applied at the inlet and outlet for the flow field [28,38]:

$$\begin{aligned} \tilde{f}_1 &= \tilde{f}_3 + \frac{2}{3}\rho_{in}u_{in}\tilde{f}_5 = \tilde{f}_7 + \frac{1}{2}(\tilde{f}_4 - \tilde{f}_2) + \frac{1}{6}\rho_{in}u_{in}\tilde{f}_8 \\ &= \tilde{f}_6 - \frac{1}{2}(\tilde{f}_4 - \tilde{f}_2) + \frac{1}{6}\rho_{in}u_{in} \end{aligned} \tag{19}$$

$$\begin{aligned} \tilde{f}_3 &= \tilde{f}_1 - \frac{2}{3}\rho_{out}u_{out}\tilde{f}_7 = \tilde{f}_5 - \frac{1}{2}(\tilde{f}_4 - \tilde{f}_2) - \frac{1}{6}\rho_{out}u_{out} - \frac{1}{2}\rho_{out}v_{out}\tilde{f}_6 \\ &= \tilde{f}_8 + \frac{1}{2}(\tilde{f}_4 - \tilde{f}_2) - \frac{1}{6}\rho_{out}u_{out} + \frac{1}{2}\rho_{out}v_{out} \end{aligned} \tag{20}$$

By using Eqs. (21) and (22) for the thermal boundary conditions at inlet and outlet, the unknown distribution functions at these sections can be calculated, respectively [23]:

$$\begin{aligned} \tilde{g}_5 &= \frac{6\rho e + 3dt\sum_i f_i Z_i - 6(\tilde{g}_0 + \tilde{g}_2 + \tilde{g}_3 + \tilde{g}_4 + \tilde{g}_6 + \tilde{g}_7)}{2 + 3u_{in} + 3u_{in}^2} \\ &\quad \times [3.0 + 6u_{in} + 3.0u_{in}^2]\frac{1}{36}\tilde{g}_1 \\ &= \frac{6\rho e + 3dt\sum_i f_i Z_i - 6(\tilde{g}_0 + \tilde{g}_2 + \tilde{g}_3 + \tilde{g}_4 + \tilde{g}_6 + \tilde{g}_7)}{2 + 3u_{in} + 3u_{in}^2} \\ &\quad \times [1.5 + 1.5u_{in} + 3.0u_{in}^2]\frac{1}{9}\tilde{g}_8 \\ &= \frac{6\rho e + 3dt\sum_i f_i Z_i - 6(\tilde{g}_0 + \tilde{g}_2 + \tilde{g}_3 + \tilde{g}_4 + \tilde{g}_6 + \tilde{g}_7)}{2 + 3u_{in} + 3u_{in}^2} \\ &\quad \times [3.0 + 6u_{in} + 3.0u_{in}^2]\frac{1}{36} \end{aligned} \tag{21}$$

$$\tilde{g}_6 = \frac{6(\tilde{g}_1+\tilde{g}_5+\tilde{g}_8)-3dt\sum_i\left(\frac{c_{ix}}{c}\right)Z_i f_i - 6\rho e u_{out}}{2-3u_{out}+3u_{out}^2} \times\left[3.0-6.0u_{out}+6.0v_{out}+3.0u_{out}^2+3.0v_{out}^2-9.0u_{out}v_{out}\right]\frac{1}{36}\tilde{g}_3$$
$$= \frac{6(\tilde{g}_1+\tilde{g}_5+\tilde{g}_8)-3dt\sum_i\left(\frac{c_{ix}}{c}\right)Z_i f_i - 6\rho e u_{out}}{2-3u_{out}+3u_{out}^2} \times\left[1.5-1.5u_{out}+3.0u_{out}^2-1.50v_{out}^2\right]\frac{1}{9}\tilde{g}_7$$
$$= \frac{6(\tilde{g}_1+\tilde{g}_5+\tilde{g}_8)-3dt\sum_i\left(\frac{c_{ix}}{c}\right)Z_i f_i - 6\rho e u_{out}}{2-3u_{out}+3u_{out}^2} \times\left[3.0-6.0u_{out}-6.0v_{out}+3.0u_{out}^2+3.0v_{out}^2+9.0u_{out}v_{out}\right]\frac{1}{36} \quad (22)$$

The slip velocity and temperature jump boundary conditions would be simulated by the specular reflective bounce back model (combination of bounce back and specular boundary condition) and diffuse scattering boundary condition (DSBC), respectively [40,44]. For example, the unknown distribution functions along the nanochannel bottom wall are stated as:

$$\tilde{f}_2 = \tilde{f}_4 \quad (23\text{-}1)$$

$$\tilde{f}_{5,6} = r\tilde{f}_{7,8} + (1-r)\tilde{f}_{8,7} \quad (23\text{-}2)$$

where r represents the accommodation coefficient. In the following and for the unknown distribution functions of temperature jump along the nanochannel bottom wall:

$$\tilde{g}_{2,5,6} = \frac{3}{\rho_w e} g^e_{2,5,6}(\rho_w, \mathbf{u}_w, e_w)(\tilde{g}_4+\tilde{g}_7+\tilde{g}_8) \quad (24)$$

Naturally the slip velocity and temperature jump along on the nanochannel top wall are simulated similarly.

3.3. Rarefaction and thermal creeping effects

In the nanochannels, the influence of compressibility and rarefaction in the slip flow regime should be involved. Tangential temperature gradients along the nanochannel walls might lead to begin the rarefied gas flows so that the fluid begins creeping in the way from cold place toward hot one. This phenomenon is called thermal creeping or transpiration [3].

According to the several fundamental works of Maxwell [8] and von Smoluchowski [9] over on dynamic of gases, the slip velocity and temperature jump can be demonstrated as follows:

$$u_{gas}-u_{wall} = \lambda\frac{2-\sigma_v}{\sigma_v}\frac{\partial u}{\partial y}\bigg|_{wall} + \frac{3}{4}\frac{\mu}{\rho T_{gas}}\frac{\partial T}{\partial x}\bigg|_{wall} T_{gas}-T_{wall}$$
$$= \frac{2-\sigma_T}{\sigma_T}\frac{2k}{k+1}\frac{\lambda}{\mathrm{Pr}}\frac{\partial T}{\partial y}\bigg|_{wall} \quad (25)$$

σ_v, σ_T are the tangential momentum and temperature accommodation coefficients. Dimensionless forms of previous equations are derived using characteristic velocity of $u_0=u_i$ and temperature $T_0=T_C$, respectively [1,3]:

$$U_s = U_{gas}-U_{wall} = \mathrm{Kn}\frac{2-\sigma_v}{\sigma_v}\frac{\partial U}{\partial Y}\bigg|_{wall} + \frac{3}{2\pi}\frac{k-1}{k}\frac{\mathrm{Kn}^2\mathrm{Re}}{\mathrm{Ec}}\frac{\partial\theta}{\partial X}\bigg|_{wall}\theta_s$$
$$= \left|\theta_{gas}-\theta_{wall}\right| = \frac{2-\sigma_T}{\sigma_T}\frac{2k}{k+1}\frac{Kn}{\mathrm{Pr}}\frac{\partial\theta}{\partial Y}\bigg|_{wall} \quad (26)$$

where $\sigma_v=\sigma_T=1$, $\mathrm{Ec}=\frac{u_0^2}{c_p\Delta T}=(k-1)T_0\mathrm{Ma}^2/\Delta T$ and $\Delta T=T_{gas}-T_0$ are supposed at this work. The second term in right hand side of Eq. (26) represents the thermal creeping phenomenon which appears to be $O(\mathrm{Kn}^2)$. So this term is usually ignored to determine the slip velocity. However this article claims that it may be important in the nanochannels with tangential temperature gradients on their surfaces.

Moreover, the tangential temperature gradient is supposed by the prescribed heat flux over the nanochannel surfaces in the literature. In the contrary, present study aims to show the existence and even also significant effects of thermal creeping in a nanochannel with constant temperature over its walls. Eventually the local and averaged Nusselt numbers (Nu_X and Nu_m) along the nanochannel walls are stated as:

$$\mathrm{Nu}_X = \left(\frac{\partial\theta}{\partial Y}\right)_{Y=0,Y=1}, \quad \mathrm{Nu}_m = \frac{1}{L}\int_0^L \mathrm{Nu}_X\, dX \quad (27)$$

4. Validations

The flow and heat transfer of the air nanoflow is simulated using the LBM developed computer code in FORTRAN language. Appropriate grid independency study is performed between 1050×35, 1200×40 and 1350×45 lattice nodes; and among them the lattice with 1200×40 nodes shows suitable accuracy and is chosen for the further calculations.

In Fig. 3, the fully developed dimensionless velocity profiles ($U=u/u_i$) through a nanochannel are compared with those of Zhang et al. [31] at $\mathrm{Kn}=0.05$ and $\mathrm{Kn}=0.1$ and suitable agreements are observed between them. To have more validation, temperature profiles of $\theta=T/T_{\mathrm{inlet}}$ at different cross sections of a nanochannel versus the results of Kavehpour et al. [7] are presented in Fig. 4 for $\mathrm{Re}=0.01$, $T_{wall}=10$, $T_{inlet}=1$, $\mathrm{Pr}=0.7$ and $\mathrm{Kn}_{in}=0.01$; This figure also shows good agreements.

5. Results and discussions

Forced convection of air in a two dimensional nanochannel is studied numerically by using lattice Boltzmann method (Fig. 1). Nanochannel side walls are kept hot while the cold inlet air

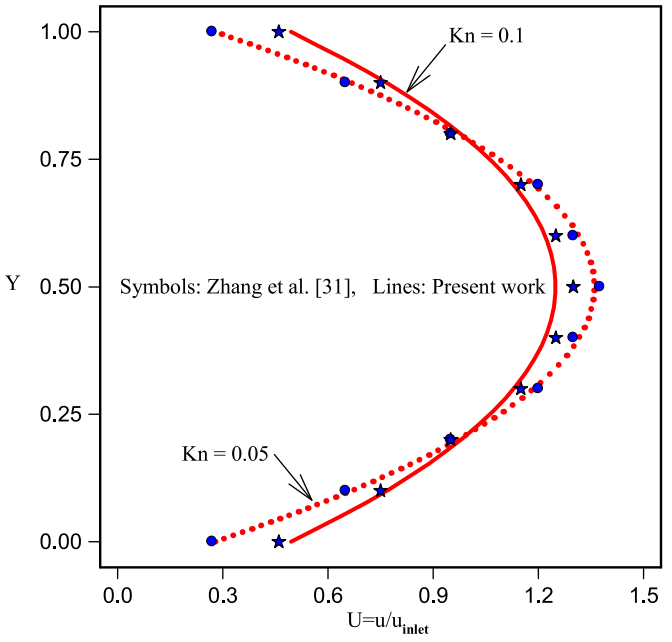

Fig. 3. Fully developed velocity profiles through a channel versus those of Zhang et al. [31].

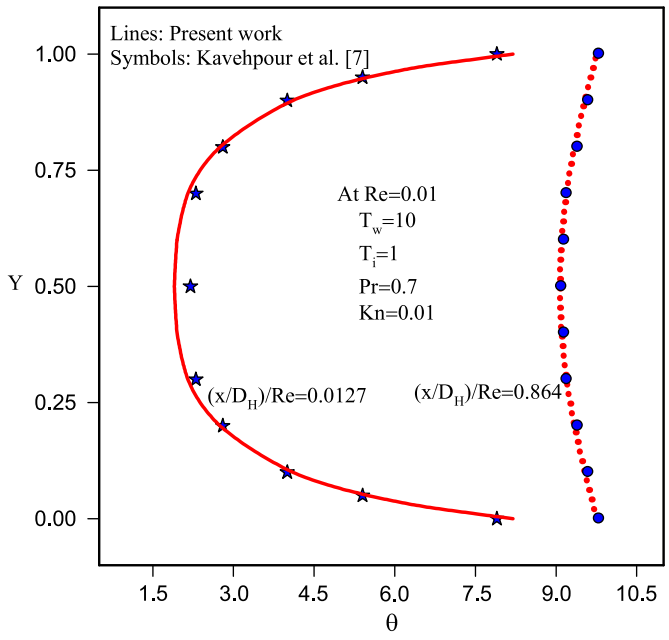

Fig. 4. Comparison of temperature profiles, $\theta=T/T_i$, through a channel with those of Kavehpour et al. [7].

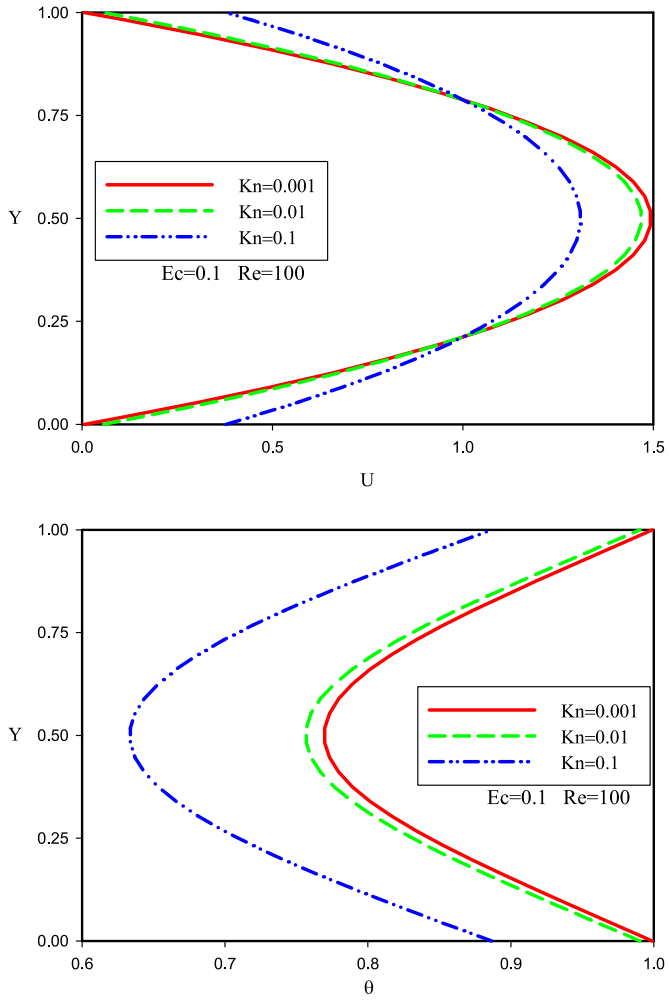

Fig. 5. Fully developed dimensionless horizontal velocity profiles, U, and dimensionless temperature profiles, θ, along the vertical centerline of nanochannel at Ec=0.1 and Re=100 for different values of Kn.

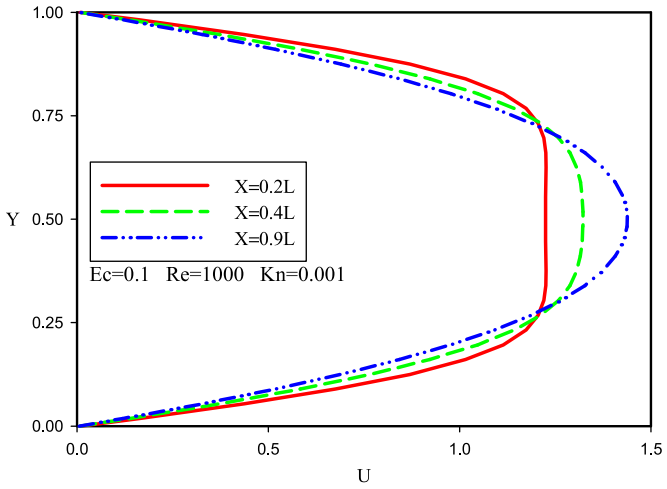

Fig. 6. Profiles of U along the nanochannel at Ec=0.1, Re=1000 and Kn=0.001.

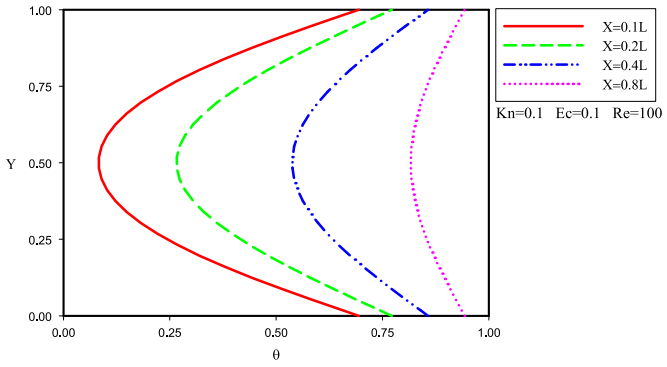

Fig. 7. Profiles of θ along the nanochannel at Kn=0.1, Ec=0.1 and Re=100.

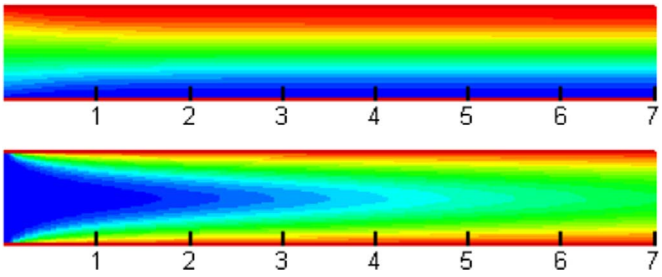

Fig. 8. Streamlines (top) and Isotherms (bottom) at Re=100, Kn=0.01 and Ec=0.1.

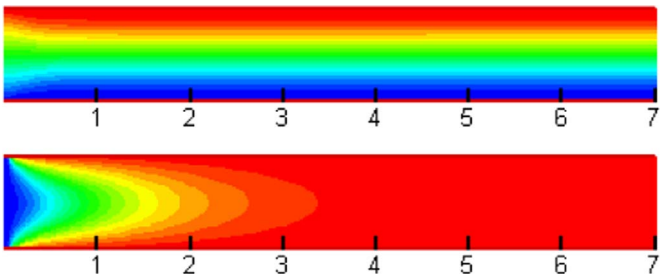

Fig. 9. Streamlines (top) and Isotherms (bottom) at Re=10, Kn=0.01 and Ec=0.1.

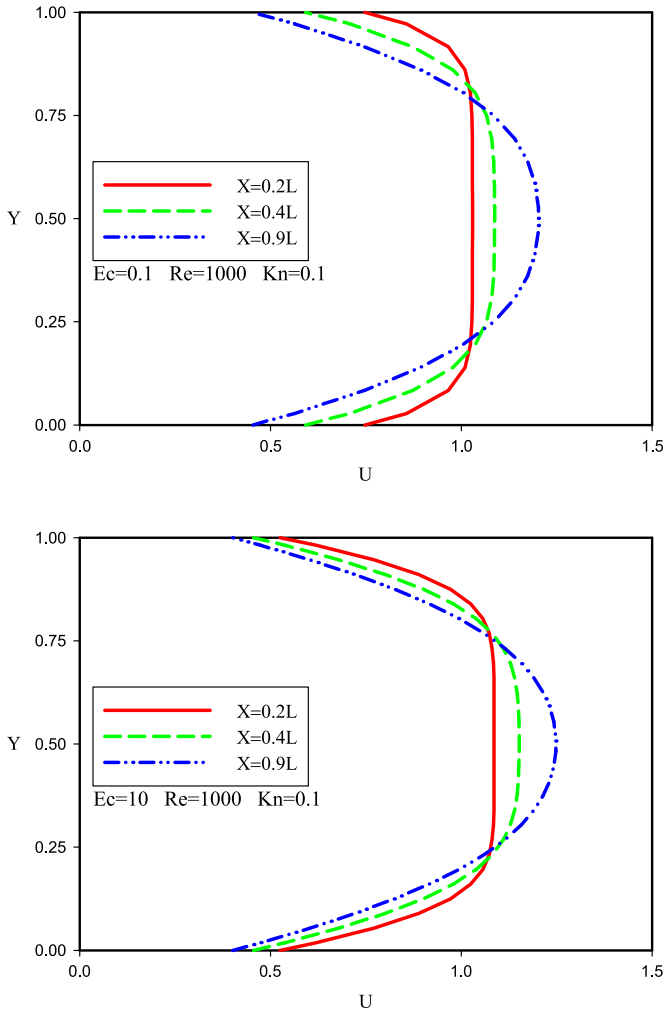

Fig. 10. The effects of Ec on U profiles along the nanochannel at Re=1000 and Kn=0.1.

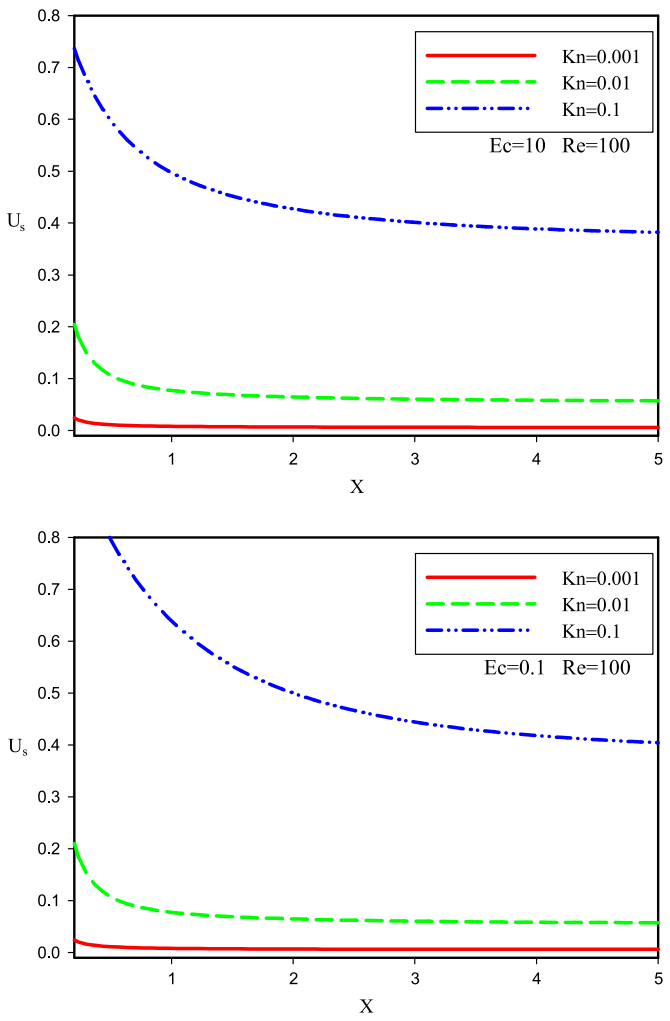

Fig. 11. Dimensionless slip velocity, U_s, along the nanochannel wall at different values of Ec and Kn for Re=100.

streams along them; moreover its aspect ratio is equals to AR=L/H=30.

5.1. Effects of Knudsen and Reynolds number

The fully developed dimensionless horizontal velocity profiles, $U=u/u_i$, and dimensionless temperature profiles, $\theta=(T-T_C)/(T_H-T_C)$, along the vertical centerline of nanochannel at Ec=0.1 and Re=100 for different values of Kn are shown in Fig. 5. For the state of Kn=0.001 which almost implies to the continuum regime, the maximum of U occurs at horizontal centerline (at Y=0.5) with the amount of U_{max}=1.5 with ignorable slip velocity adjacent to the walls (at Y=0 and Y=1). More Kn corresponds to more slip at these areas which leads to less U_{max}. In the other hand, higher Kn causes lower values for θ near the walls and on the horizontal centerline that mean less heat exchange between the fluid and walls.

Fig. 6 illustrates the variations of U profiles at different cross sections along the nanochannel at Ec=0.1, Re=1000 and Kn=0.001. The fully developed condition would occur later at more values of Re as well as X=0.9L where this condition has not been achieved yet in. So it can be mentioned that in the state of Re=1000, the whole nanochannel domain is under developing (not fully developed) where the most temperature gradient between the air and walls existences. In the following, the inlet air warming up due to heat exchange with the hot walls is reported in Fig. 7 which concerned at Kn=0.1, Ec=0.1 and Re=100.

Figs. 8 and 9 present the streamlines and isotherms for Kn=0.01 and Ec=0.1 at Re=100 and Re=10, respectively. Streamlines are completely smooth and symmetric along the horizontal centerline except in a small place at entrance region of left hand side of nanochannel. Fig. 9 shows that the whole space of nanochannel (for $X>3.5$) is almost in thermal equilibrium with the walls at Re=10 while the isotherms of Fig. 8 related to Re=100, do not follow such this process; so more length is needed to achieve the isothermal condition.

5.2. Effects of Eckert number

Fig. 10 shows the effects of Ec on U profiles along the nanochannel at Re=1000 and Kn=0.1. It is observed that Ec affects the velocity profiles significantly at adjacent to walls in entrance region (see the plots related to X=0.2L); so that U profiles far from the inlet do not change sensible with Ec .

Variations of dimensionless slip velocity, U_s, along the nanochannel wall at different values of Ec and Kn for Re=100 are provided in Fig. 11. U_s begins from its maximum amount at inlet and then decreases along the nanochannel so that it tends to a constant value at fully developed part of nanochannel. More focus implies that how important is the effect of Ec on U_s for the state of Kn=0.1 (at $X<4$); as well as less value of Ec corresponds to more U_s. The both effects of Re and Ec on the profiles of U_s are presented

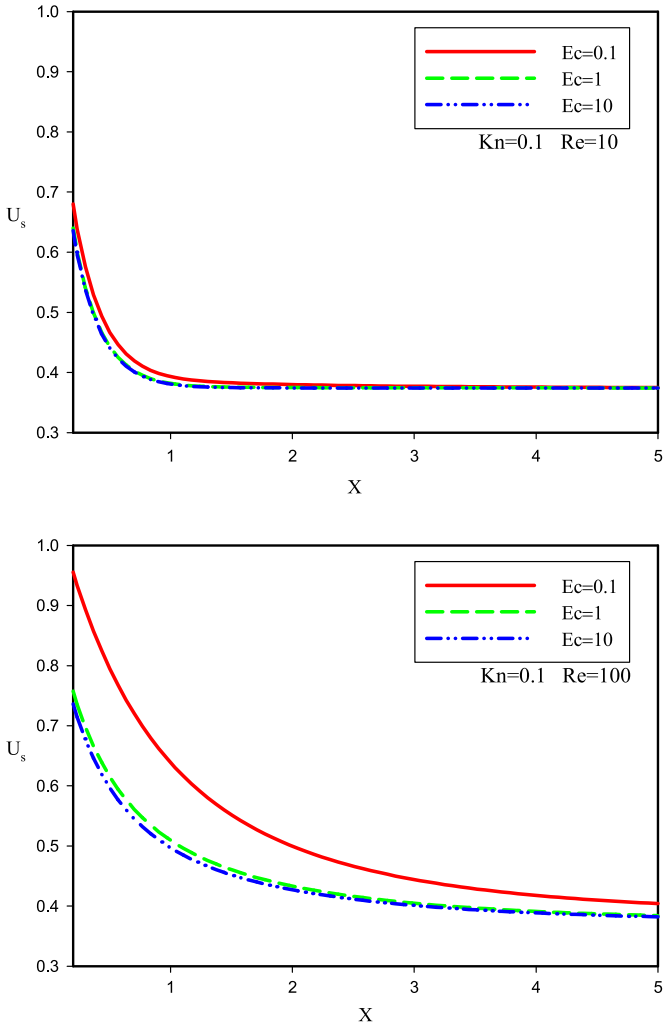

Fig. 12. The effects of Ec and Re on slip velocity along the nanochannel wall at Kn=0.1.

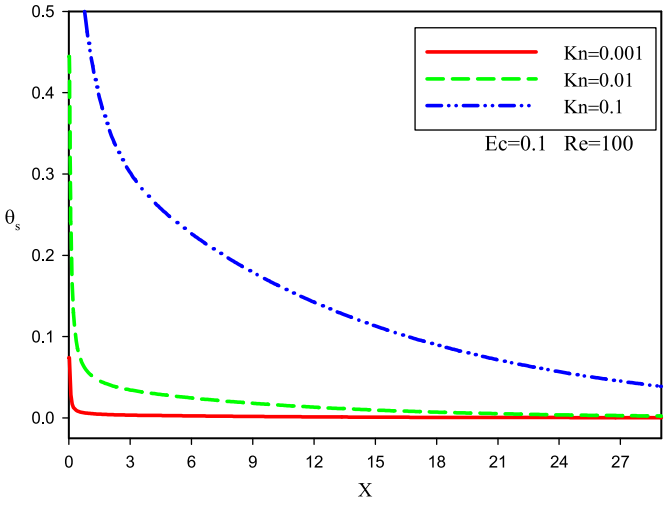

Fig. 13. Dimensionless temperature jump, θ_s, along the nanochannel wall at different values of Kn.

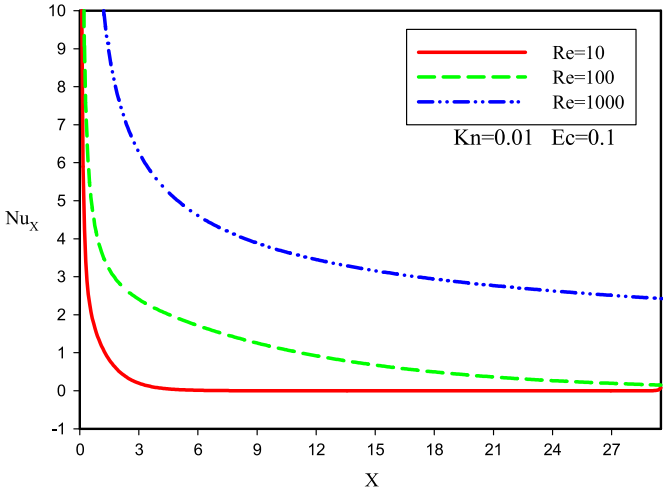

Fig. 14. Nu_X along the nanochannel wall at different values of Re.

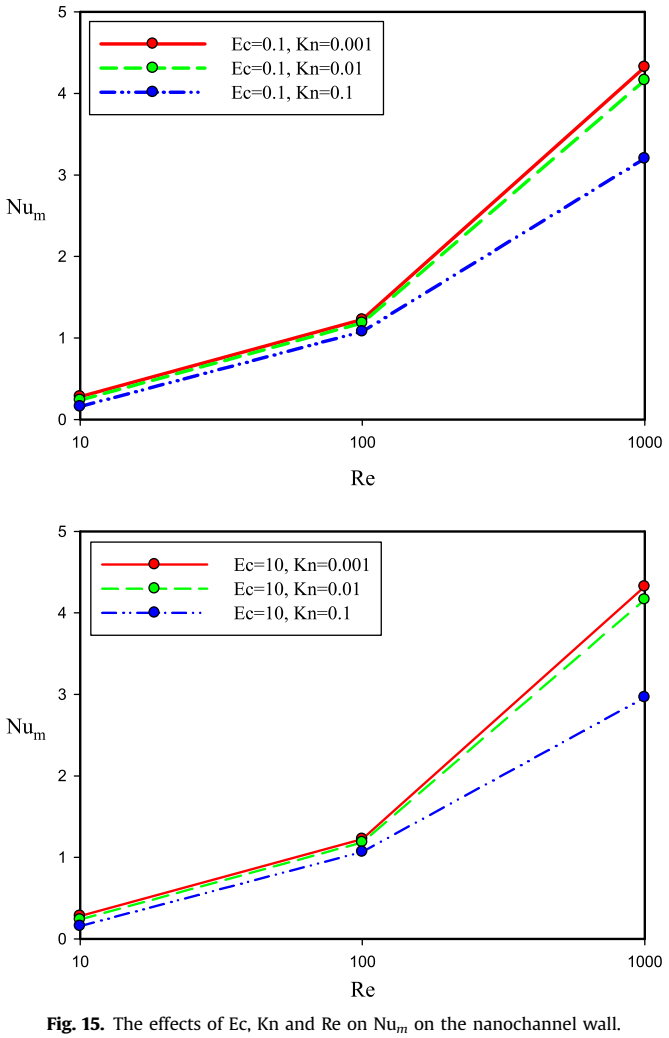

Fig. 15. The effects of Ec, Kn and Re on Nu_m on the nanochannel wall.

in Fig. 12. As it is said the lower amount of Ec would correspond to a higher value of U_s; although this fact occurs more severely at Re=100 than the mode of Re=10. Moreover the results concerned Ec=10 and Ec=1 are more similar to one another than those of Ec=0.1. It is worth noting that the negative effect of Ec on U_s is more sensible at larger Kn.

The higher values of temperature jump, θ_s, are achieved at entrance region where the most temperature gradient between the cold air and hot wall exists (see Fig. 13). Along the nanochannel, flow approaches to the isothermal pattern with increasing the heat exchange; so the amount of θ_s would be

negligible far from the inlet. However θ_s increases with Kn which means more length will be required to become fully developed. Moreover the positive effect of Re to increase the local Nusselt number (Nu_X) and thermal entrance length can be obviously traced in Fig. 14.

Eventually the values of averaged Nusselt number (Nu_m) versus all of Kn, Ec and Re are seen in Fig. 15. Higher Re and lower Kn increase Nu_m and also the effects of Ec can be ignored on. However the lowering effect of Kn is more significant at Kn=0.1 than the states of Kn=0.001 and Kn=0.01.

6. Conclusion

Forced convection of air in a two dimensional nanochannel was studied numerically by using the lattice Boltzmann method. Nanochannel side walls were kept hot while the cold inlet air streamed along them. The calculations were performed for Re=10,100,1000 and Kn=0.001,0.01,0.1 and Ec=0.1,1,10. The effects of slip flow regime (according to Kn) involved thermal creeping (according to Ec) on hydrodynamic and thermal domains were investigated for the first time by the lattice Boltzmann method and the following points were achieved:

1. Thermal creeping was usually ignored to determine the slip velocity in the literature. However this article showed that it might be so important in a nanochannel with tangential temperature gradient on its surface.
2. The tangential temperature gradient was practically supposed by the prescribed heat flux over the solid surfaces. In the contrary, the thermal creeping significant effects were observed clearly at present study in a nanochannel with constant temperature over its walls which meant the temperature jump phenomenon would be able to generate the thermal creeping motion.
3. More Knudsen number (Kn) corresponded to more slip velocity (U_s) and temperature jump (θ_s) and less Nusselt number (Nu). It also significantly increased the entrance length.
4. Lower amount of Ec led to higher value of U_s. Although the results concerned Ec=10 and Ec=1 were more similar to one another than those of Ec=0.1. It was worth noting that the inverse effect of Ec on U_s was more sensible at larger Kn. Moreover Ec affected significantly the slip velocity in entrance region so that U profiles far from the inlet did not change sensible with Ec.
5. The mentioned effects of Ec and Kn on hydrodynamic and thermal domains were severely invigorated at higher values of Reynolds number.
6. According to Eq. (26); thermal creeping strength depends on Kn^2Re/Ec. Based on this work results, it is recommended that thermal creeping effects for the range of $Ec \leq 0.1$, $Kn \geq 0.1$ and $Re \geq 100$ take in to account and be included, especially for hydrodynamic properties.

References

[1] N.T. Nguyen, S.T. Wereley, Fundamentals and Applications of Microfluidics, Second ed., Artech House Inc., Norwood, MA, 2006.
[2] M.H. Esfe, M. Akbari, D. Toghraie, A. Karimipour, M. Afrand, Effect of nanofluid variable properties on mixed convection flow and heat transfer in an inclined two-sided lid-driven cavity with sinusoidal heating on sidewalls, Heat Transf. Res. 45 (2014) 409–432.
[3] G. Karniadakis, A. Beskok, N. Alura, Microflows and Nanoflows Fundamentals and Simulation, Springer, New York, 2005.
[4] M.H. Esfe, A.A.A. Arani, A. Karimipour, S.S.M. Esforjani, Numerical simulation of natural convection around an obstacle placed in an enclosure filled with different types of nanofluids, Heat Transf. Res. 45 (2014) 279–292.
[5] A. Karimipour, A.H. Nezhad, A. Behzadmehr, S. Alikhani, E. Abedini, Periodic mixed convection of a nanofluid in a cavity with top lid sinusoidal motion, Proc. Inst. Mech. Eng. Part C: J. Mech. Eng. Sci. 225 (2011) 2149–2160.
[6] K. Han, Y.T. Feng, D.R.J. Owen, Modelling of thermal contact resistance within the framework of the thermal lattice Boltzmann method, Int. J. Therm. Sci. 47 (2008) 1276–1283.
[7] H.P. Kavehpour, M. Faghri, Y. Asako, Effects of compressibility and rarefaction on gaseous flows in microchannels, Numer. Heat Transf. Part A 32 (1997) 677–696.
[8] J.C. Maxwell, On stresses in rarefied gases arising from inequalities of temperature, Philos. Trans. R. Soc. Part 1 170 (1879) 231–256.
[9] V.M. Smoluchowski, Ü ber Wärmeleitung in verdünnten Gasen, Ann. Phys. Chem. (1898) 101–130.
[10] M. Gad-el-Hak, Flow physics in MEMS, Mécanique & Industries 2 (4) (2001) 313–341.
[11] C. Chang, Y.T. Yang, T.H. Yen, C.K. Chen, Numerical investigation into thermal mixing efficiency in Y-shaped channel using lattice Boltzmann method and field synergy principle, Int. J. Therm. Sci. 48 (2009) 2092–2099.
[12] Z. Hashemi, O. Abouali, R. Kamali, Thermal three-dimensional Lattice Boltzmann simulations of suspended solid particles in microchannels, Int. J. Heat Mass Transf. 65 (2013) 235–243.
[13] E.S. Oran, C.K. Oh, B.Z. Cybyk, Direct simulation Monte Carlo: recent advances and applications, Ann. Rev. Fluid Mech. 30 (1998) 403–441.
[14] W.A. Zahid, Y. Yin, K. Zhu, Couette–Poiseuille flow of a gas in long microchannels, Microfluid. Nanofluid. 3 (2007) 55–64.
[15] S. Succi, The Lattice Boltzmann equation for Fluid Dynamics and beyond, Oxford University Press, Oxford, 2001.
[16] G.A. Bird, Molecular Gas Dynamics and the Direct Simulation of Gas Flows, 1994.
[17] J. Wang, L. Chen, Q. Kang, S.S. Rahman, The lattice Boltzmann method for isothermal micro-gaseous flow and its application in shale gas flow: a review, Int. J. Heat Mass Transf. 95 (2016) 94–108.
[18] Y.H. Qian, D. d'Humieres, P. Lallemand, Lattice BGK models for Navier–Stokes equation, Europhys. Lett. 17 (1992) 479–484.
[19] S. Chen, Z. Tian, Simulation of microchannel flow using the lattice Boltzmann method, Physica 388 (2009) 4803–4810.
[20] W.C. Hung, Y. Ru, A numerical study for slip flow heat transfer, Appl. Math. Comput. 173 (2006) 1246–1264.
[21] A. Karimipour, A.H. Nezhad, A. D'Orazio, E. Shirani, Investigation of the gravity effects on the mixed convection heat transfer in a microchannel using lattice Boltzmann method, Int. J. Therm. Sci. 54 (2012) 142–152.
[22] A. D'Orazio, M. Corcione, G.P. Celata, Application to natural convection enclosed flows of a lattice Boltzmann BGK model coupled with a general purpose thermal boundary condition, Int. J. Therm. Sci. 43 (2004) 575–586.
[23] C. Zhang, F. Hong, P. Cheng, Simulation of liquid thin film evaporation and boiling on a heated hydrophilic microstructured surface by lattice Boltzmann method, Int. J. Heat Mass Transf. 86 (2015) 629–638.
[24] A. D'Orazio, S. Succi, C. Arrighetti, Lattice Boltzmann simulation of open flows with heat transfer, Phys. Fluids 15 (2003) 2778–2781.
[25] X. Nie, G.D. Doolen, S. Chen, Lattice-Boltzmann simulation of fluid flows in MEMS, J. Stat. Phys. 107 (2002) 279—289.
[26] S. Chen, Lattice Boltzmann method for slip flow heat transfer in circular microtubes: extended Graetz problem, Appl. Math. Comput. 217 (2010) 3314–3320.
[27] C.Y. Lim, C. Shu, X.D. Niu, Y.T. Chew, Application of lattice Boltzmann method to simulate microchannel flows, Phys. Fluids 14 (2002) 2299–2308.
[28] Q. Zou, X. He, On pressure and velocity boundary conditions for the lattice Boltzmann BGK model, Phys. Fluids 9 (1997) 1591–1599.
[29] P.L. Bhatnagar, E.P. Gross, M. Krook, A model for collision process in gases. I. Small amplitude processes in charged and neutral one-component system, Phys. Rev. 94 (1954) 511–522.
[30] A. Karimipour, A.H. Nezhad, A. D'Orazio, M.H. Esfe, M.R. Safaei, E. Shirani, Simulation of copper–water nanofluid in a microchannel in slip flow regime using lattice Boltzmann method, Eur. J. Mech. B/Fluids 49 (2015) 89–99.
[31] Y.H. Zhang, R.S. Qin, Y.H. Sun, R.W. Barber, D.R. Emerson, Gas flow in microchannels – a lattice Boltzmann method approach, J. Stat. Phys. 121 (2005) 257–267.
[32] A. Karimipour, New correlation for Nusselt number of nanofluid with Ag/Al_2O_3/Cu nanoparticles in a microchannel considering slip velocity and temperature jump by using lattice Boltzmann method, Int. J. Therm. Sci. 91 (2015) 146–156.
[33] X. He, S. Chen, G.D. Doolen, A novel thermal model for the lattice Boltzmann method in incompressible limit, J. Comput. Phys. 146 (1998) 282–300.
[34] Z.W. Tian, C. Zou, H.J. Liu, Z.L. Guo, Z.H. Liu, C.G. Zheng, Lattice Boltzmann scheme for simulating thermal micro-flow, Physica 385 (2007) 59–68.
[35] F.H. Lai, Y.T. Yang, Lattice Boltzmann simulation of natural convection heat transfer of Al_2O_3/water nanofluids in a square enclosure, Int. J. Therm. Sci. 50 (2011) 1930–1941.
[36] A. Karimipour, A.H. Nezhad, A. D'Orazio, E. Shirani, The effects of inclination angle and Prandtl number on the mixed convection in the inclined lid driven cavity using lattice Boltzmann method, J. Theor. Appl. Mech. 51 (2) (2013) 447–462.
[37] A. Karimipour, M.H. Esfe, M.R. Safaei, D.T. Semiromi, S. Jafari, S.N. Kazi, Mixed convection of copper–water nanofluid in a shallow inclined lid driven cavity using the lattice Boltzmann method, Physica A 402 (2014) 150–168.
[38] A.A. Alamyane, A.A. Mohamad, Simulation of forced convection in a channel

with extended surfaces by the lattice Boltzmann method, Comput. Math. Appl. 59 (2010) 2421–2430.
[39] X.D. Niu, C. Shu, Y.T. Chew, A lattice Boltzmann BGK model for simulation of micro flows, Europhys. Lett. 67 (4) (2004) 600–606.
[40] X.D. Niu, C. Shu, Y.T. Chew, A thermal lattice Boltzmann model with diffuse scattering boundary condition for micro thermal flows, Comput. Fluids 36 (2007) 273–281.
[41] C. Shu, X.D. Niu, Y.T. Chew, A lattice Boltzmann kinetic model for microflow and heat transfer, J. Stat. Phys. 121 (2005) 239–255.
[42] L. Szalmas, Multiple-relaxation time lattice Boltzmann method for the finite Knudsen number region, Physica 379 (2007) 401–408.
[43] Y. Gao, Using MRT lattice Boltzmann method to simulate gas flow in simplified catalyst layer for different inlet–outlet pressure ratio, Int. J. Heat Mass Transf. 88 (2015) 122–132.
[44] F. Verhaeghe, L.S. Luo, B. Blanpain, Lattice Boltzmann modeling of microchannel flow in slip flow regime, J. Comput. Phys. 228 (2009) 147–157.
[45] M. Baratpour, A. Karimipour, M. Afrand, S. Wongwises, Effects of temperature and concentration on the viscosity of nanofluids made of single-wall carbon nanotubes in ethylene glycol., Inst. Commun. Heat Mass Transfer 74 (2016) 108–113.
[46] H. Babovsky, A numerical model for the Boltzmann equation with applications to micro flows, Comput. Math. Appl. 58 (2009) 791–804.
[47] C. Qi, L. Liang, Z. Rao, Study on the flow and heat transfer of liquid metal based nanofluid with different nanoparticle radiuses using two-phase lattice Boltzmann method, Int. J. Heat Mass Transf. 94 (2016) 316–326.
[48] T. Zhang, D. Che, Double MRT thermal lattice Boltzmann simulation for MHD natural convection of nanofluids in an inclined cavity with four square heat sources, Int. J. Heat Mass Transf. 94 (2016) 87–100.